Title

Regional quantification of cerebral venous oxygenation from MRI susceptibility during hypercapnia

Authors

Fan, Audrey P
Evans, Karleyton C
Stout, Jeffrey N
et al.

Publication Date

2015

DOI

10.1016/j.neuroimage.2014.09.068

Peer reviewed

Published in final edited form as:
Neuroimage. 2015 January 1; 0: 146–155. doi:10.1016/j.neuroimage.2014.09.068.

Regional quantification of cerebral venous oxygenation from MRI susceptibility during hypercapnia

Audrey P Fan[1,2], **Karleyton C Evans**[1,3], **Jeffrey N Stout**[2,4], **Bruce R Rosen**[2,4], and **Elfar Adalsteinsson**[1,2,4]

Karleyton C Evans: kcevans@partners.org; Jeffrey N Stout: jstout@mit.edu; Bruce R Rosen: bruce@nmr.mgh.harvard.edu; Elfar Adalsteinsson: elfar@mit.edu

[1]Electrical Engineering and Computer Science, Massachusetts Institute of Technology, 77 Massachusetts Avenue, Cambridge, MA, USA

[2]Radiology, Athinoula A. Martinos Center for Biomedical Imaging, 149 Thirteenth Street, Charlestown, MA, USA

[3]Psychiatry, Massachusetts General Hospital East, 149 Thirteenth Street, Charlestown, MA, USA

[4]Harvard-MIT Health Sciences and Technology, Institute of Medical Engineering and Science, Massachusetts Institute of Technology, 77 Massachusetts Avenue, Cambridge, MA, USA

Abstract

There is an unmet medical need for noninvasive imaging of regional brain oxygenation to manage stroke, tumor, and neurodegenerative diseases. Oxygenation imaging from magnetic susceptibility in MRI is a promising new technique to measure local venous oxygen extraction fraction (OEF) along the cerebral venous vasculature. However, this approach has not been tested *in vivo* at different levels of oxygenation. The primary goal of this study was to test whether susceptibility imaging of oxygenation can detect OEF changes induced by hypercapnia, via CO_2 inhalation, within selected *a priori* brain regions.

Ten healthy subjects were scanned at 3 tesla with a 32-channel head coil. The end-tidal CO_2 ($ETCO_2$) was monitored continuously and inspired gases were adjusted to achieve steady-state conditions of eucapnia (41 ± 3 mmHg) and hypercapnia (50 ± 4 mmHg). Gradient echo phase images and pseudo-continuous arterial spin labeling (pcASL) images were acquired to measure regional OEF and CBF respectively during eucapnia and hypercapnia. By assuming constant cerebral oxygen consumption throughout both gas states, regional CBF values were computed to predict the local change in OEF in each brain region.

Hypercapnia induced a relative decrease in OEF of -42.3% in the straight sinus, -39.9% in the internal cerebral veins, and approximately -50% in pial vessels draining each of the occipital, parietal, and frontal cortical areas. Across volunteers, regional changes in OEF correlated with

Corresponding author: Audrey Fan, SM, Department of Electrical Engineering and Computer Science, Massachusetts Institute of Technology, 32 Vassar Street, Room 36-776, Cambridge, MA 02139, USA, apfan@mit.edu.

changes in $ETCO_2$. The reductions in regional OEF (via phase images) were significantly correlated ($P < 0.05$) with predicted reductions in OEF derived from CBF data (via pcASL images). These findings suggest that susceptibility imaging is a promising technique for OEF measurements, and may serve as a clinical biomarker for brain conditions with aberrant regional oxygenation.

Keywords

oxygenation imaging; oxygen extraction fraction; hypercapnia; quantitative susceptibility

1. Introduction

Under normal conditions, the healthy human brain receives 15% of the cardiac output and consumes 20% of total oxygen used by the body (Gallagher et al., 1998; Magistretti and Pellerin, 1996). There is an unmet clinical need for a neuroimaging method to provide repeated, non-invasive and reliable measures of regional brain oxygen utilization. Such measurements could inform pathophysiological models and target therapies in brain disorders with aberrant regional oxygenation, such as stroke (Geisler et al., 2006) and tumor (Elas et al., 2003); as well as in neurodegenerative disorders with more subtle metabolic changes such as Alzheimer's disease (Hock et al., 1997) and multiple sclerosis (Ge et al., 2012). Although there is a clinical need for robust and reliable measurements of brain oxygen utilization, previous approaches have proven to be technically challenging *in vivo*.

Positron emission tomography (PET) provides regional quantification of brain oxygen extraction fraction (OEF) and the cerebral metabolic rate of oxygen consumption ($CMRO_2$) through use of ^{15}O tracers. However, the need for high-cost specialized equipment, radiation exposure, and invasive arterial sampling limit the clinical utility of ^{15}O PET. Several magnetic resonance imaging (MRI) methods have been recently proposed to quantify cerebral oxygenation from magnetic susceptibility (Fan et al., 2012; Rodgers et al., 2013), T_2 relaxation measurements in venous blood (Krishnamurthy et al., 2013; Lu and Ge, 2008), and calibrated blood-oxygen-level-dependent (BOLD) signal changes (Bulte et al., 2012; Gauthier et al., 2012). T_2-relaxation-under-spin tagging (TRUST) MRI provides measures of cerebral OEF through estimates of T_2 relaxation of venous blood in large veins, e.g. the superior sagittal sinus (SSS). Although TRUST has been validated against pulse oximetry (Lu et al., 2012) and optimized for reproducible, fast measurements of OEF (Liu et al., 2013), the technique is limited to global measures of oxygen extraction. Our group recently proposed a method to map absolute OEF along the cerebral venous vasculature from quantitative susceptibility mapping (QSM) reconstructions (Fan et al., 2013). This susceptibility-based approach inherently provides measures of regional cerebral OEF information within individual vessels, but remains to be tested in different oxygenation states as induced by common physiological challenges.

Carbon dioxide (CO_2) is an effective vasodilator and offers an ideal cerebrovascular intervention to test the oxygenation venography method. Hypercapnia, via inhalation of 5% to 7% CO_2, causes significant vascular changes to the brain. These changes include robust increases to cerebral blood flow (CBF) ranging from 35% to 50% (Kety and Schmidt, 1948;

Sicard and Duong, 2005); increased cerebral blood volume (Ito et al., 2003); and higher blood concentrations of CO_2 and O_2. Hypercapnia has been considered a purely vascular challenge in that small or negligible changes in the cerebral metabolic rate of oxygen consumption ($CMRO_2$), a surrogate for neural activity, have been observed in studies of hypercapnia despite dramatic cerebrovascular modulations (Chen and Pike, 2010). This effect has been demonstrated by invasive studies (Kety and Schmidt, 1948) as well as non-invasive imaging studies (van Zijl et al., 1998), and is supported by Fick's principle of arterio-venous difference that implies $CMRO_2$ is proportional to CBF and to OEF.

The assumption of constant $CMRO_2$ during hypercapnia forms the basis for previous studies of: 1) cerebrovascular reserve (Bright et al., 2011; de Boorder et al., 2004), i.e. the reactivity of vessels to the gas challenge, as a measure of hemodynamic health; and 2) calibration of the BOLD signal to estimate changes in $CMRO_2$ during a functional task (Bulte et al., 2009; Davis et al., 1998). In addition, several BOLD MRI studies have indirectly observed minimal changes in $CMRO_2$ during hypercapnia (Rostrup et al., 2000; Sicard et al., 2003), which implies a decrease in OEF proportional to the increase in CBF during hypercapnia. Thus, hypercapnia reliably produces a predictable, global change in brain oxygenation that is detectable on MRI images with sensitivity to magnetic susceptibility. For instance, venous vessels appear dark due to the presence of paramagnetic deoxyhemoglobin (dHb) molecules on susceptibility-weighted images (SWI), and the loss of vessel contrast observed during hypercapnia is consistent with lower dHb concentration and decreased OEF (Rauscher et al., 2005; Sedlacik et al., 2008). Jain et al. went further to directly measure field shifts induced by the underlying changes in dHb concentration during hypercapnia from 2-dimensional, susceptibility-weighted phase images (Jain et al., 2011). This study quantified a 13% absolute decrease in OEF from the SSS during hypercapnia relative to baseline scans, demonstrating the utility of MRI susceptibility to noninvasively image global oxygenation state. However, Jain et al. did not examine regional OEF and the authors did not compare their observed OEF changes to expected increases in CBF during hypercapnia.

The primary aim of the present study was to test whether our approach, which measures oxygenation-dependent susceptibility shifts in cerebral veins (Fan et al., 2013), can detect the expected OEF changes that accompany the cerebrovascular responses to hypercapnia. We acquired 3-dimensional gradient echo volumes for quantitative susceptibility mapping (QSM) reconstruction of OEF along cerebral vessels during eucapnia and hypercapnia in young, healthy subjects at 3 tesla. Additional quantitative CBF maps were acquired using established pseudo-continuous arterial spin labeling MRI techniques (Wu et al., 2007). Assuming no change in $CMRO_2$ during mild hypercapnia, regional changes in perfusion were used to predict local oxygenation changes for comparison with QSM-based OEF measurements in veins draining different brain regions.

2. Materials and methods

2.1. MRI acquisitions

Imaging data were acquired in ten healthy subjects (six males and four females, aged 24 to 31 years) on a Siemens 3 tesla Tim Trio system with a 32-channel head receive coil. No subjects had a history of neurological, cardiopulmonary, or psychiatric illness. All subjects

gave written consent under the approval of the local institutional review board. Blood hematocrit (Hct), the percent of erythrocytes in blood, was measured from a fingerprick sample in each subject (HemoPoint H2 model #3008-0031-6801, Stanbio Laboratory Inc., Bourne, TX). At the start of each experiment, we acquired a structural magnetization-prepared rapid acquisition (MEMPR) sequence (van der Kouwe et al., 2008) in the sagittal orientation with repetition time (TR) = 2530 ms; echo time (TE) = 3.5 ms; inflow time = 900 ms; resolution = 1.0 × 1.0 × 1.0 mm^3; matrix size = 256 × 256 × 176; flip angle (FA) = 9° bandwidth (BW) = 190 Hz/pixel; and R = 2 parallel imaging acceleration (Griswold et al., 2002) for an acquisition time (TA) of 6 minutes.

Following the anatomical scan, subjects were placed on a breathing apparatus (described below) and imaged during each of two gas conditions, eucapnia and hypercapnia. Gradient echo (GE) phase images were acquired for susceptibility mapping to measure OEF along brain venous vasculature, and pseudo-continuous arterial spin labeling (pcASL) scans were acquired to measure perfusion in the deep gray matter and cortical tissue. The order of MRI acquisitions was counterbalanced between the two conditions to avoid order-dependent bias effects.

The 3-dimensional, dual-echo GE scans were flow-compensated along all spatial axes (Deistung et al., 2009) with TR = 23 ms; TE = 7.2, 17.7 ms; resolution = 0.875 × 0.875 × 1.0 mm^3; matrix size = 256 × 224 × 144; FA = 15°; BW = 260 Hz/pixel; partial Fourier (PF) = 6/8; and R = 2 acceleration for TA of ∼6 minutes. During the eucapnic state, we also acquired three low-resolution, single-echo GE scans with the same spatial coverage to assist with coil combination of the high-resolution GE data. These scans were acquired with TR = 23 ms; TE = 6-8 ms; resolution = 1.8 × 1.8 × 2.0 mm^3; matrix size = 128 × 112 × 72; FA = 15°, BW = 260 Hz/pixel; PF = 6/8; and R = 2 acceleration for TA of ∼1 minute per echo. Uncombined magnitude and phase images were saved for all GE acquisitions.

The 2-dimensional ASL scans were acquired with TR = 3500 ms; TE = 13 ms; resolution = 3.4 × 3.4 × 6.0 mm^3; labeling duration = 1500 ms; post-label delay = 1200 ms; R = 2 acceleration; and 40 control-tag pairs for a total TA of ∼4 minutes. During each condition, a separate calibration scan was acquired to map M_{0T}, the fully relaxed longitudinal magnetization of local tissue, for calibration of quantitative CBF values. The parameters of the calibration scan included TR = 8000; TE = 13 ms; resolution = 3.4 × 3.4 × 6.0 mm^3; labeling duration = 1500 ms; post-label delay = 5000 ms; R = 2 acceleration; and 4 averages for TA of ∼1 minute.

2.2. Gas manipulations

Resting baseline end-tidal CO_2 ($ETCO_2$) was measured via nasal cannula during the MEMPR scan with an MRI-compatible capnograph (Capstar-100, CWE Inc., Ardmore, PA). After the MEMPR scan, subjects subsequently breathed through a mouthpiece attached to a specialized breathing circuit designed to maintain end-tidal gases (PO_2 and PCO_2) within ±2 mmHg of target values despite changes in ventilation (Banzett et al., 2000; McKay et al., 2003). The subject's nose was sealed with medical tape to ensure that all ventilation occurred via the breathing circuit. The circuit comprised the mouthpiece (with an integrated $ETCO_2$ sample port) connected in series to a heat moisture exchanger (AirLife® HEPA

Filter, CareFusion, San Diego, CA); a pneumotach to measure airway flow and compute tidal volume (ADInstruments MTL300, Colorado Springs, CO); followed by a Y-shaped non-rebreathing valve (Hans Rudolph, Inc. #2630, Shawnee, KS). The non-rebreathing valve was configured to permit a limited supply of investigator-controlled gas through one inlet (controlled gas limb) and allow re-inspired alveolar gas through the other inlet (alveolar gas limb) when ventilation exceeded the investigator-controlled gas flow. To minimize subject motion, the mouthpiece was secured to top portion of the head receive coil.

Gases were delivered from tanks containing medical air, 7% carbon dioxide with balance medical air, and 100% oxygen (Airgas Inc., Radnor, PA). Gas flows were adjusted via a digital flow-meter (Sierra Instruments, FloBox™ 954, L Monterey, CA) to achieve the desired gas mixtures. Subjects received 30% O_2 and 70% N_2 during the eucapnic condition. This mixture was adjusted during the hypercapnic condition to target an 8-mmHg increase in $ETCO_2$ relative to baseline in each subject (30% O_2, 5 – 6.5% CO_2, balance N_2). The mixture was designed for slight hyperoxia, which induces mild vasoconstriction, to counteract the vasodilation created by the increased CO_2 content in the gas. Hyperoxia has also been shown to stabilize variations in $ETCO_2$ caused by potential hyperventilation (Bulte et al., 2007; Poulin et al., 1998).

While on the breathing circuit, $ETCO_2$ was monitored continuously in each subject via capnograph (Capstar-100) and the airway flow signal was monitored by a spirometer (ADInstruments, Spirometer FE141, Colorado Springs, CO). Physiological signals were recorded to computer disk with an analog-to-digital data acquisition system (Powerlab 16/30, ADInstruments, Colorado Springs, CO). The $ETCO_2$ curves were calibrated by accounting for the expired partial pressure of water vapor (47 mmHg) (Severinghaus, 1989) and barometric pressure on the day of the experiment. Figure 1 depicts representative time courses of $ETCO_2$ and minute ventilation throughout the experiment from a typical subject.

2.3. Data analysis

2.3.1. Quantitative susceptibility mapping reconstruction—Phase images were combined from individual channel magnitude and phase volumes after correcting for spatial RF offsets in each receive channel, as described in (Fan et al., 2013). After coil combination, all phase images were spatially unwrapped in 3D by the FSL Prelude software (Jenkinson, 2003), constrained by a brain mask defined from the GE magnitude images with the FSL Brain Extraction Tool (Smith, 2002). Unreliable voxels with non-linear phase evolution across TE were identified and were not considered in later processing steps (Schweser et al., 2011a). Phase image processing was performed independently for images acquired during eucapnia and hypercapnia. For each gas condition, a field map estimate (in ppm) was calculated as $b = \phi_{TE2}/(\gamma \cdot TE_2 \cdot B_0)$. Global background fields were estimated by 100 iterations of the projection onto dipole fields (PDF) routine (Liu et al., 2011) and subsequently removed, resulting in a local field map for input into the QSM algorithm.

Various QSM approaches have been proposed to recover the underlying susceptibility values in cerebral veins, including thresholded k-space deconvolution (Haacke et al., 2010), multi-orientation sampling of phase images (Schweser et al., 2011b), and mathematical regularization of single-orientation phase images (Liu et al., 2012; Xu et al., 2013). In this

study, we adopted a rapid split-Bregman solver for QSM reconstruction with regularization via a total variation (TV) penalty (Bilgic et al., 2013). The TV regularization term promotes a sparse number of nonzero spatial gradients in χ, such that the optimal χ is favored to be piecewise constant within anatomical tissue boundaries. Because the split-Bregman reconstruction approach is relatively fast, the optimal weighting parameter (λ_{TV}) for the TV regularization term was automatically selected for each gas condition separately. This optimal λ_{Tv} weighting ranged from 7×10^{-4} to 9×10^{-4}, and typically did not differ between eucapnic and hypercapnic scans.

2.3.2. Processing of arterial spin labeling scans—The pcASL time series were visually inspected to confirm the absence of severe motion artifacts (≤ 3.5 mm inter-scan movement) and realigned in SPM8 to correct for subtle subject movement (Friston et al., 2007). For each gas condition, quantitative CBF maps in ml/100g/min were generated from the average difference signal (ΔM) between control and tag images after simple subtraction, through the following relationship (Buxton et al., 1998):

$$CBF = \frac{6000 \cdot \lambda \cdot \Delta M \cdot e^{PLD/T_{1,blood}}}{2 \cdot \alpha \cdot T_{1,blood} \cdot M_{0T} \cdot (1 - e^{-\tau/T_{1,blood}})} \quad [1]$$

where λ = 0.9 ml/g is the blood-brain partition coefficient (Herscovitch and Raichle, 1985); PLD = 1200 ms is the post-label delay of the tag; $T_{1,blood}$ = 1650 ms is the relaxation constant of arterial blood at 3 tesla (Lu et al., 2004); α = 0.95 and α = 0.84 are the labeling efficiency for pcASL acquisitions during eucapnia and hypercapnia, respectively (Aslan et al., 2010); M_{0T} is the longitudinal magnetization of tissue from the calibration scan; and τ = 1500ms is labeling duration of the scan. For CBF quantification, PLD was adjusted per imaging slice to account for the slice acquisition time of 37.5 ms.

2.3.3. Quantitative measurements of brain physiology—To guide local physiological measurements, Freesurfer (http://surfer.nmr.mgh.harvard.edu) was used to reconstruct cortical parcellations from the anatomical MEMPR data in each subject (Dale et al., 1999; Fischl et al., 1999). The cortical segmentation was registered to the QSM maps and to the CBF maps with nearest-neighbor interpolation within SPM8 (Friston et al., 2007).

For each gas state, venous blood susceptibility was measured in the following *a priori* vessels: straight sinus, internal cerebral veins, and in pial vessels draining the occipital, parietal, and frontal lobes (Figure 2). These veins were selected because they are relatively large compared to the acquired voxel size and are well-described in imaging literature of venographic methods (Leach et al., 2006). To avoid potential partial volume effects, only voxels in the highest 20^{th} percentile of susceptibility values per vessel were considered in the OEF analysis for each gas condition. Across subjects, an average of 7.9 ± 3 voxels per vessel were identified for pial veins, 18.1 ± 8 voxels for the internal cerebral veins, and 34.6 ± 9 for the straight sinus. Venous susceptibility was referenced to that of cerebrospinal fluid (CSF), as estimated from a region of interest (ROI) with volume 140 ± 39 mm^3 in the anterior portion of the ventricles. The susceptibility difference between each vein and CSF

($\Delta\chi_{\text{vein-CSF}}$) was then calibrated to quantitative, local OEF in absolute percentage points as follows (Haacke et al., 1997; Weisskoff and Kiihne, 1992):

$$\Delta\chi_{\text{vein}-\text{CSF}} = OEF \cdot \Delta\chi_{\text{do}} \cdot Hct + \Delta\chi_{\text{oxy}-\text{water}} \cdot Hct \quad [2]$$

where $\Delta\chi_{\text{do}}$ = 0.27 ppm is the susceptibility shift per unit hematocrit between fully oxygenated and fully deoxygenated erythrocytes (Jain et al., 2012); $\Delta\chi_{\text{oxy-water}}$ = -0.03 ppm is the susceptibility shift between oxygenated blood cells and water (Weisskoff and Kiihne, 1992); and *Hct* was measured in each subject.

Regional CBF values during eucapnia and during hypercapnia were determined from gray matter tissue ROIs in the deep gray matter, thalamus, occipital cortex, parietal cortex, and frontal cortex, as depicted in Figure 3. These ROIs were defined by the Freesurfer cortical segmentation, and only voxels with greater than 50% probability of assignment to gray matter were included in CBF measurements. Local CBF values averaged within the ROIs were then used to predict the expected OEF change in veins draining each brain region.

2.3.4. OEF predictions from blood flow changes—Assuming that $CMRO_2$ is constant in each gas state, and applying Fick's principle of arteriovenous difference,

$$CMRO_{2,H} = CMRO_{2,E} \quad [3]$$

$$CBF_H \cdot OEF_H = CBF_E \cdot OEF_E \quad [4]$$

$$OEF_H = \frac{CBF_E}{CBF_H} \cdot OEF_E \quad [5]$$

where the subscript “H” indicates hypercapnia and the subscript “E” indicates eucapnia. If regional CBF values for a given brain area are known, the predicted normalized change in local OEF is:

$$\frac{|\Delta OEF|}{OEF_E} = \frac{|OEF_H - OEF_E|}{OEF_E} = \left(\frac{CBF_H}{CBF_E}\right) - 1 \quad [6]$$

Note that the OEF predictions are based solely on the ASL measurements of CBF, and are evaluated against measured OEF changes from independent susceptibility acquisitions.

2.3.5. Statistical methods—Quantitative OEF and CBF were compared between eucapnic and hypercapnic conditions using a paired student *T*-test across subjects. We used Pearson correlation coefficients to test whether normalized changes in local OEF related to $\Delta ETCO_2$ during the gas challenge. To compare predicted versus normalized changes in local OEF, we used the Pearson correlation ($P < 0.05$) and also created a *T*-statistic (*T* = measured slope/standard error of the slope) to test whether the slope was statistically different from 1.

3. Results

3.1. Physiological measurements of CBF and OEF during eucapnia and hypercapnia

The group mean of hematocrit values was 41.6 ± 4 (SD)%. Hypercapnia increased the subjects' $ETCO_2$ from 41.3 ± 3 mmHg to 49.9 ± 4 mmHg and increased minute ventilation from 9.9 ± 2 L/min to 24.0 ± 6 L/min, corresponding to a hypercapnic ventilatory response of 1.6 ± 0.6 L/min per mmHg. The breathing circuit facilitated stable levels of $ETCO_2$ during each gas condition (Figure 1). From the gradient echo acquisition, diminished contrast in veins, consistent with decreased susceptibility of venous blood, was observed during hypercapnia relative to eucapnia both on magnitude and QSM images (Figure 2).

Group mean quantitative CBF and OEF values for selected *a priori* brain regions are reported for each gas condition in Table 1. As expected, robust increases in CBF were observed during hypercapnia relative to eucapnia (*P*-values < 0.001); with 64.5 ± 22% relative CBF increase in deep gray matter, and increases of 69.0% to 89.7% in CBF across cortical ROIs. Large decreases in vessel OEF were also observed during hypercapnia relative to eucapnia (*P*-values < 0.001). Specifically, a -42.3 ± 15% relative OEF decrease was measured from the straight sinus, and approximately -50% decreases in OEF were observed in pial vessels draining the different cortical regions.

Linear correlations for group data were observed between percent ΔOEF and $\Delta ETCO_2$ for each brain regions included in the analysis (Figure 4); all *P*-values < 0.05. The slope of this linear relationship was similar across most brain areas and ranged from 6.5% to 7.5% per mmHg, except in the parietal cortex, for which the slope was 3.7% per mmHg.

3.2. Comparison of measured versus predicted OEF change in various brain regions

The observed % change in OEF from susceptibility acquisitions linearly correlated with predicted % change in OEF from CBF measurements for the group. This relationship was observed both in deep gray matter regions (Figure 5a) and in more superficial cortical regions (Figure 5b); all *P*-values < 0.03. The slope of the linear fit between predicted and measured % OEF for nearly all brain regions was close to, albeit slightly above, identity. These slope values ranged between 1.11 and 1.43 except for the parietal cortex (with fitted slope of 0.62); although none of the slopes were statistically different from 1 within our sample.

4. Discussion

The present study demonstrates the first MRI-based non-invasive approach to provide reliable measures of regional brain oxygen utilization. Susceptibility measurements from flow-compensated GE scans revealed large decreases in OEF during hypercapnia. We demonstrated robust OEF reductions in five brain areas, including three distinct cortical regions, in which the decreases in OEF significantly correlated with independent perfusion measures obtained from an established pcASL imaging technique.

4.1. Vessel contrast during gas modulation

Consistent with previous hypercapnia studies (Gauthier et al., 2011; Rauscher et al., 2005; Sedlacik et al., 2008), we observed attenuation of venous contrast on the GE magnitude images during hypercapnia relative to baseline. This change in contrast was driven by a decrease in dHb content, and thus a decrease in χ within brain vessels, which was also observed on the QSM maps reconstructed from the GE phase images. Importantly, the QSM maps are quantitative and self-referenced to χ values in the CSF, such that the vessel signal intensity is not influenced by T_1 relaxation or field inhomogeneity profiles. These factors may allow for changes in venous contrast to be more apparent on QSM images (Figure 1b) compared to magnitude images (Figure 1a).

4.2. Regional OEF changes during hypercapnia

We measured strong reductions of local venous OEF during hypercapnia relative to baseline within individual vessels. For instance, OEF decreased by ~40% in the straight sinus and in the internal cerebral veins draining the deep gray matter; and decreased by over 50% in pial veins draining specific cortical territories. The magnitude of OEF reductions observed in the present study are comparable with the hypercapnia-mediated OEF decrease of 42.6% in the SSS observed by Xu et al. via TRUST MRI (Xu et al., 2011). However, substantially smaller OEF changes due to hypercapnia were observed in other studies: Sedlacik et al. reported a 18.4% OEF reduction in the straight sinus (Sedlacik et al., 2008) via GE magnitude images, and Jain et al. reported a 20% OEF reduction in the SSS via GE phase images (Jain et al., 2011). The variance in oxygenation changes during hypercapnia between studies may be explained by differences in 1) $ETCO_2$ levels during the gas modulation; (2) fraction of inspired O_2 (FiO_2); and (3) baseline measurement of absolute OEF, which varied from 24% to 36% across different image acquisition and processing strategies. Since there were large differences in breathing circuits used across studies, we suggest that between-study differences $ETCO_2$ levels served as the greatest source of variance in the reported ΔOEF values.

Although we targeted the same $\Delta ETCO_2$ elevation in each individual, subjects exhibited slightly different ventilatory responses, and consequently modest differences in $\Delta ETCO_2$ during the hypercapnic intervention. Across subjects, the $\Delta ETCO_2$ was tightly correlated with the % change in OEF reductions in each brain region (Figure 4). The slope of these relationships characterizes the cerebrovascular reactivity (CVR) of vessels, and we observed a 6.2 ± 1% change in OEF per 1 mmHg increase of $ETCO_2$ across the brain. If oxygen metabolism is constant in both gas states, the magnitude of the OEF response is expected to be similar to the perfusion response (per 1 mmHg increase in $ETCO_2$) during hypercapnia. In fact, the CVR computed from our susceptibility-based OEF values is in line with CVR computed from MRI flow in previous hypercapnia studies. For instance, Jain et al. observed a CVR of 6.1%/mmHg from phase-contrast flow measurements in major cerebral arteries (Jain et al., 2011); although other studies have reported slightly lower values for CVR (~3%/mmHg) from ASL perfusion measurements in gray matter during hypercapnia (Heijtel et al., 2014; Villien et al., 2013).

As an independent measure of the hemodynamic response to hypercapnia, pcASL perfusion maps were also collected in each gas state. Regional CBF values were used to predict the OEF change expected in brain vessels associated with each brain region, assuming no change in $CMRO_2$. OEF reductions during hypercapnia correlated with predicted OEF changes in all brain regions investigated for this study. This provides compelling evidence that our method derives physiologically meaningful estimates of local, cerebral venous OEF that are coupled to regional CBF.

4.3. Limitations

The findings in the present study should be considered in the context of the following limitations. An important assumption for OEF predictions in the current study is that $CMRO_2$ remains unchanged between eucapnia and mild hypercapnia. This assumption is supported by invasive studies (Kety and Schmidt, 1948) and imaging studies in healthy adults. These imaging studies combined oxygenation estimates in the SSS (Jain et al., 2011) or in the jugular veins of the neck (Chen and Pike, 2010) with flow measurements, and found no change in global $CMRO_2$ during mild hypercapnia. However, one recent MRI study found that breathing CO_2 led to 13% suppression of global $CMRO_2$ (Xu et al., 2011). In the context of our study, a small decrease in $CMRO_2$ could be driven by a greater OEF reduction than predicted from underlying CBF increases. There may have been evidence of these effects in the present study, as seen in the plot of measured versus predicted OEF changes (Figure 5), in cases for which the slope was greater than 1. However, this trend was not observed consistently across brain regions, at least within the measurement error of our experiments.

The pairing between vessels (identified on the GE images) and the brain regions corresponding to their drainage (delineated by structural ROIs overlaid on the CBF maps) in this work was relatively coarse. Venous blood drainage from the brain is less stereotyped than the arterial system and there is no validated technique to determine this drainage pattern *in vivo*, especially on the scale of the pial veins identified here (∼2mm in diameter). Furthermore, although hypercapnia is generally considered to affect the brain in a global manner, regional variations have been reported. (Kastrup et al., 1999). If the vascular response to hypercapnia follows a predictable spatial pattern across the brain, careful identification of the drainage territory on CBF maps would be necessary to accurately predict the local OEF change in each vessel. This consideration also has implications for potential clinical use of susceptibility imaging in vessels. Although our approach may identify abnormal OEF in specific veins from patients, the exact corresponding brain tissue region remains unknown, especially if the venous drainage is disrupted by pathology. To define the appropriate tissue ROI for vessels in patients, future work could develop noninvasive imaging of venous territories in the brain, e.g. via the spin-labeling MRI approach proposed by (Wong and Guo, 2013).

We adopted a pcASL labeling scheme to compute regional CBF values in order to predict the OEF change expected in brain vessels associated with each brain region. Although the pcASL protocol in the present study was similar to those used successfully in previous studies (Chen et al., 2011; Xu et al., 2010), these techniques are still under development. For

instance, we assumed a lower labeling efficiency for pcASL during hypercapnia relative to eucapnia, due to the higher flow velocity in feeding arteries during CO_2 inhalation (Aslan et al., 2010). However, the assumed labeling efficiency value of 0.95 during eucapnia is slightly higher than other values in the literature (Dai et al., 2008). It is unclear whether this discrepancy is due to mild hyperventilation while subjects were on the mouthpiece or due to physiological differences between subject cohorts in these studies. Potential CBF quantification errors may have added variance to our OEF predictions, such that the R-value of the linear fits between predicted and measured OEF were lower than expected.

In the present study, minute ventilation increased by ∼14 L/min during hypercapnia relative to baseline. This change is comparable with a previously reported 13.4 L/min increase of minute ventilation in 14 healthy subjects during inhalation of gas with 7% CO_2 (Somers et al., 1989). The resultant hypercapnia ventilatory response of 1.6 L/min per mmHg is also physiologically reasonable, compared to literature values ranging between 1.69 and 2.69 L/min per mmHg (Banzett et al., 1996; Hirshman et al., 1975; Kikuchi et al., 1994; Weil et al., 1975). Elevated ventilation may create increase subject movement during the gas manipulations, although the maximum displacement observed during SPM realignment of our pCASL scans was not different between eucapnia (0.26 ± 0.3 mm) and hypercapnia (0.29 ± 0.2 mm). Potential alterations to blood pressure, heart rate, and oxygenation itself due to the ventilation increase may have also contributed to variance in both OEF measurements and predictions.

4.4. Future methodological improvements to oxygenation imaging from susceptibility

For this investigation, we focused on normalized OEF changes $(\frac{|\Delta OEF|}{OEF_E})$ measured by MRI susceptibility instead of absolute OEF during hypercapnic intervention. This OEF metric was selected because it is less vulnerable to absolute quantification errors, which may occur due to partial volume effects and flow-induced phase artifacts that persist despite flow compensation in the GE acquisitions. These secondary flow artifacts occur due to moving blood spins through an inhomogeneous susceptibility field gradient, and can lead to nearly 30% overestimation in absolute OEF if uncorrected (Xu et al., 2013). For instance, the SSS is a large draining vessel with a relatively fast flow of 280 mL/min (Jordan et al., 1994). Its geometry and orientation with respect to the magnetic field gradient is also more complex than the straight sinus. For these reasons, the SSS did not appear uniform in contrast as expected in the 3-dimensional QSM maps, and it was challenging to reliably measure OEF in the SSS from susceptibility images.

In the absence of quantification biases, absolute $CMRO_2$ could theoretically be computed via the Fick principle from OEF and CBF values for each gas condition (Fan et al., 2012; Kety and Schmidt, 1948). With our raw OEF measurements, $CMRO_2$ would decrease by 30%, from 121 ± 15 μmol/100g/min during eucapnia to 86 ± 15 μmol/100g/min during hypercapnia across subjects. This $CMRO_2$ reduction is much greater than previous imaging reports. After correction for 30% overestimation in OEF due to flow artifacts (Xu et al., 2013), however, $CMRO_2$ would only decrease by 10% from 167 ± 17 μmol/100g/min during eucapnia to 150.8 ± 15 μmol/100g/min during hypercapnia. This reduction is not

significant and is more in line with the literature (Chen and Pike, 2010; Jain et al., 2012). We note that the corrected values for absolute $CMRO_2$ are also more consistent with ^{15}O PET measurements in the cortex (Ibaraki et al., 2008; Ishii et al., 1996). This analysis suggests that secondary flow effects may contaminate the quantification of OEF and $CMRO_2$ in pial vessels and need to be addressed before absolute OEF measurements can be validated for use in the clinic.

To achieve sufficient resolution for local OEF measurement from small vessels, our GE scans required a 6-min acquisition time in each gas state, throughout which the cerebral physiology of interest presumably remained stable. This acquisition is several times longer than global oxygenation measurements such as TRUST MRI (1:12 minutes) (Xu et al., 2011) or phase susceptometry measurements in the SSS (22 seconds) (Jain et al., 2011). The long acquisition time limits the number of echoes that can be collected in one scan, especially since long flow compensation waveforms between echoes are necessary for reliable χ estimation in vessels. As such, our method would benefit from more efficient sampling trajectories, such as spirals (Wu et al., 2012), to collect GE phase images at multiple (more than three) echoes in a reasonable scan time. A multi-echo, fast acquisition would improve the accuracy of χ estimates, enable the modeling and removal of flow artifacts on phase images, and facilitate application of the oxygenation measurement technique in clinical settings.

4.4. Conclusions

This study demonstrates a novel, non-invasive approach to measure regional cerebral OEF from quantitative susceptibility MRI. Robust OEF changes in individual veins were observed during hypercapnia relative to eucapnia. Furthermore, the measured OEF changes in each brain region correlated with predictions of OEF changes derived from independent measures of perfusion (CBF), providing confidence in the fidelity of oxygenation measures from QSM reconstructions. Although the OEF imaging approach was tested via hypercapnia, use of the method in practice does not require gas manipulations to provide baseline OEF measurements. MR susceptibility imaging of OEF is a reliable, quantitative technique that holds great promise as a clinical biomarker. In particular, non-invasive measures of regional cerebral oxygenation could potentially enhance the management of stroke and tumor, and inform pathophysiological models of neurodegenerative diseases.

Acknowledgments

Audrey Fan is supported by a training grant from the National Institute of Biomedical Imaging and Bioengineering (T32-EB001680). Dr. Karleyton Evans is supported by a grant from the National Institute of Health (K23-MH086619) and he discloses grant support from Pfizer Ltd., unrelated to the present study. Dr. Bruce Rosen would like to acknowledge the following affiliation: Department of Meridian & Acupuncture, East-West Medical Research Institute and School of Korean Medicine, Kyung Hee University, Republic of Korea. We thank Dr. David Boas for helpful insight into experimental design and Dr. Louis Gagnon for suggestions to improve the manuscript. Dr. Berkin Bilgic provided instrumental support toward the quantitative susceptibility analyses utilized in this work.

References

Aslan S, Xu F, Wang PL, Uh J, Yezhuvath US, van Osch M, Lu H. Estimation of labeling efficiency in pseudocontinuous arterial spin labeling. Magn Reson Med. 2010; 63:765–771. [PubMed: 20187183]

Banzett RB, Garcia RT, Moosavi SH. Simple contrivance “clamps” end-tidal PCO(2) and PO(2) despite rapid changes in ventilation. J Appl Physiol (1985). 2000; 88:1597–1600. [PubMed: 10797118]

Banzett RB, Lansing RW, Evans KC, Shea SA. Stimulus-response characteristics of CO2-induced air hunger in normal subjects. Respir Physiol. 1996; 103:19–31. [PubMed: 8822220]

Bilgic B, Fan AP, Polimeni JR, Cauley SF, Bianciardi M, Adalsteinsson E, Wald LL, Setsompop K. Fast quantitative susceptibility mapping with L1-regularization and automatic parameter selection. Magn Reson Med. 2013

Bright MG, Donahue MJ, Duyn JH, Jezzard P, Bulte DP. The effect of basal vasodilation on hypercapnic and hypocapnic reactivity measured using magnetic resonance imaging. J Cereb Blood Flow Metab. 2011; 31:426–438. [PubMed: 20959855]

Bulte DP, Chiarelli PA, Wise RG, Jezzard P. Cerebral perfusion response to hyperoxia. J Cereb Blood Flow Metab. 2007; 27:69–75. [PubMed: 16670698]

Bulte DP, Drescher K, Jezzard P. Comparison of hypercapnia-based calibration techniques for measurement of cerebral oxygen metabolism with MRI. Magn Reson Med. 2009; 61:391–398. [PubMed: 19165902]

Bulte DP, Kelly M, Germuska M, Xie J, Chappell MA, Okell TW, Bright MG, Jezzard P. Quantitative measurement of cerebral physiology using respiratory-calibrated MRI. Neuroimage. 2012; 60:582–591. [PubMed: 22209811]

Buxton RB, Frank LR, Wong EC, Siewert B, Warach S, Edelman RR. A general kinetic model for quantitative perfusion imaging with arterial spin labeling. Magn Reson Med. 1998; 40:383–396. [PubMed: 9727941]

Chen JJ, Pike GB. Global cerebral oxidative metabolism during hypercapnia and hypocapnia in humans: implications for BOLD fMRI. J Cereb Blood Flow Metab. 2010; 30:1094–1099. [PubMed: 20372169]

Chen Y, Wang DJ, Detre JA. Test-retest reliability of arterial spin labeling with common labeling strategies. J Magn Reson Imaging. 2011; 33:940–949. [PubMed: 21448961]

Dai W, Garcia D, de Bazelaire C, Alsop DC. Continuous flow-driven inversion for arterial spin labeling using pulsed radio frequency and gradient fields. Magn Reson Med. 2008; 60:1488–1497. [PubMed: 19025913]

Dale AM, Fischl B, Sereno MI. Cortical surface-based analysis. I. Segmentation and surface reconstruction. Neuroimage. 1999; 9:179–194. [PubMed: 9931268]

Davis TL, Kwong KK, Weisskoff RM, Rosen BR. Calibrated functional MRI: mapping the dynamics of oxidative metabolism. Proc Natl Acad Sci U S A. 1998; 95:1834–1839. [PubMed: 9465103]

de Boorder MJ, Hendrikse J, van der Grond J. Phase-contrast magnetic resonance imaging measurements of cerebral autoregulation with a breath-hold challenge: a feasibility study. Stroke. 2004; 35:1350–1354. [PubMed: 15131315]

Deistung A, Dittrich E, Sedlacik J, Rauscher A, Reichenbach JR. ToF-SWI: simultaneous time of flight and fully flow compensated susceptibility weighted imaging. J Magn Reson Imaging. 2009; 29:1478–1484. [PubMed: 19472425]

Elas M, Williams BB, Parasca A, Mailer C, Pelizzari CA, Lewis MA, River JN, Karczmar GS, Barth ED, Halpern HJ. Quantitative tumor oxymetric images from 4D electron paramagnetic resonance imaging (EPRI): methodology and comparison with blood oxygen level-dependent (BOLD) MRI. Magn Reson Med. 2003; 49:682–691. [PubMed: 12652539]

Fan AP, Benner T, Bolar DS, Rosen BR, Adalsteinsson E. Phase-based regional oxygen metabolism (PROM) using MRI. Magn Reson Med. 2012; 67:669–678. [PubMed: 21713981]

Fan AP, Bilgic B, Gagnon L, Witzel T, Bhat H, Rosen BR, Adalsteinsson E. Quantitative oxygenation venography from MRI phase. Magn Reson Med. 2013

Fischl B, Sereno MI, Dale AM. Cortical surface-based analysis. II: Inflation, flattening, and a surface-based coordinate system. Neuroimage. 1999; 9:195–207. [PubMed: 9931269]

Friston, KJ.; Ashburner, J.; Kiebel, SJ.; Nichols, TE.; Penny, WD. Statistical parametric mapping: The analysis of functional brain images. London: 2007.

Gallagher D, Belmonte D, Deurenberg P, Wang Z, Krasnow N, Pi-Sunyer FX, Heymsfield SB. Organ-tissue mass measurement allows modeling of REE and metabolically active tissue mass. Am J Physiol. 1998; 275:E249–258. [PubMed: 9688626]

Gauthier CJ, Desjardins-Crepeau L, Madjar C, Bherer L, Hoge RD. Absolute quantification of resting oxygen metabolism and metabolic reactivity during functional activation using QUO2 MRI. Neuroimage. 2012; 63:1353–1363. [PubMed: 22986357]

Gauthier CJ, Madjar C, Tancredi FB, Stefanovic B, Hoge RD. Elimination of visually evoked BOLD responses during carbogen inhalation: implications for calibrated MRI. Neuroimage. 2011; 54:1001–1011. [PubMed: 20887792]

Ge Y, Zhang Z, Lu H, Tang L, Jaggi H, Herbert J, Babb JS, Rusinek H, Grossman RI. Characterizing brain oxygen metabolism in patients with multiple sclerosis with T2-relaxation-under-spin-tagging MRI. J Cereb Blood Flow Metab. 2012; 32:403–412. [PubMed: 22252237]

Geisler BS, Brandhoff F, Fiehler J, Saager C, Speck O, Rother J, Zeumer H, Kucinski T. Blood-oxygen-level-dependent MRI allows metabolic description of tissue at risk in acute stroke patients. Stroke. 2006; 37:1778–1784. [PubMed: 16741186]

Griswold MA, Jakob PM, Heidemann RM, Nittka M, Jellus V, Wang J, Kiefer B, Haase A. Generalized autocalibrating partially parallel acquisitions (GRAPPA). Magn Reson Med. 2002; 47:1202–1210. [PubMed: 12111967]

Haacke EM, Lai S, Reichenbach JR, Kuppusamy K, Hoogenraad FGC, Takeichi H, Lin WL. In vivo measurement of blood oxygen saturation using magnetic resonance imaging: A direct validation of the blood oxygen level-dependent concept in functional brain imaging. Hum Brain Mapp. 1997; 5:341–346. [PubMed: 20408238]

Haacke EM, Tang J, Neelavalli J, Cheng YC. Susceptibility mapping as a means to visualize veins and quantify oxygen saturation. J Magn Reson Imaging. 2010; 32:663–676. [PubMed: 20815065]

Heijtel DF, Mutsaerts HJ, Bakker E, Schober P, Stevens MF, Petersen ET, van Berckel BN, Majoie CB, Booij J, van Osch MJ, Vanbavel E, Boellaard R, Lammertsma AA, Nederveen AJ. Accuracy and precision of pseudo-continuous arterial spin labeling perfusion during baseline and hypercapnia: A head-to-head comparison with O HO positron emission tomography. Neuroimage. 2014; 92C:182–192. [PubMed: 24531046]

Herscovitch P, Raichle ME. What is the correct value for the brain--blood partition coefficient for water? J Cereb Blood Flow Metab. 1985; 5:65–69. [PubMed: 3871783]

Hirshman CA, McCullough RE, Weil JV. Normal values for hypoxic and hypercapnic ventilaroty drives in man. J Appl Physiol. 1975; 38:1095–1098. [PubMed: 1141125]

Hock C, Villringer K, Muller-Spahn F, Wenzel R, Heekeren H, Schuh-Hofer S, Hofmann M, Minoshima S, Schwaiger M, Dirnagl U, Villringer A. Decrease in parietal cerebral hemoglobin oxygenation during performance of a verbal fluency task in patients with Alzheimer's disease monitored by means of near-infrared spectroscopy (NIRS)--correlation with simultaneous rCBF-PET measurements. Brain Res. 1997; 755:293–303. [PubMed: 9175896]

Ibaraki M, Miura S, Shimosegawa E, Sugawara S, Mizuta T, Ishikawa A, Amano M. Quantification of cerebral blood flow and oxygen metabolism with 3-dimensional PET and 15O: validation by comparison with 2-dimensional PET. J Nucl Med. 2008; 49:50–59. [PubMed: 18077532]

Ishii K, Sasaki M, Kitagaki H, Sakamoto S, Yamaji S, Maeda K. Regional difference in cerebral blood flow and oxidative metabolism in human cortex. J Nucl Med. 1996; 37:1086–1088. [PubMed: 8965174]

Ito H, Kanno I, Ibaraki M, Hatazawa J, Miura S. Changes in human cerebral blood flow and cerebral blood volume during hypercapnia and hypocapnia measured by positron emission tomography. J Cereb Blood Flow Metab. 2003; 23:665–670. [PubMed: 12796714]

Jain V, Abdulmalik O, Propert KJ, Wehrli FW. Investigating the magnetic susceptibility properties of fresh human blood for noninvasive oxygen saturation quantification. Magnetic Resonance in Medicine. 2012; 68:863–867. [PubMed: 22162033]

Jain V, Langham MC, Floyd TF, Jain G, Magland JF, Wehrli FW. Rapid magnetic resonance measurement of global cerebral metabolic rate of oxygen consumption in humans during rest and hypercapnia. J Cereb Blood Flow Metab. 2011; 31:1504–1512. [PubMed: 21505481]

Jenkinson M. Fast, automated, N-dimensional phase-unwrapping algorithm. Magn Reson Med. 2003; 49:193–197. [PubMed: 12509838]

Jordan JE, Pelc NJ, Enzmann DR. Velocity and flow quantitation in the superior sagittal sinus with ungated and cine (gated) phase-contrast MR imaging. J Magn Reson Imaging. 1994; 4:25–28. [PubMed: 8148552]

Kastrup A, Kruger G, Glover GH, Neumann-Haefelin T, Moseley ME. Regional variability of cerebral blood oxygenation response to hypercapnia. Neuroimage. 1999; 10:675–681. [PubMed: 10600413]

Kety SS, Schmidt CF. The Effects of Altered Arterial Tensions of Carbon Dioxide and Oxygen on Cerebral Blood Flow and Cerebral Oxygen Consumption of Normal Young Men. J Clin Invest. 1948; 27:484–492. [PubMed: 16695569]

Kikuchi Y, Okabe S, Tamura G, Hida W, Homma M, Shirato K, Takishima T. Chemosensitivity and perception of dyspnea in patients with a history of near-fatal asthma. N Engl J Med. 1994; 330:1329–1334. [PubMed: 8152444]

Krishnamurthy LC, Liu P, Ge Y, Lu H. Vessel-specific quantification of blood oxygenation with T -relaxation-under-phase-contrast MRI. Magn Reson Med. 2013:0. [PubMed: 23568830]

Leach JL, Fortuna RB, Jones BV, Gaskill-Shipley MF. Imaging of cerebral venous thrombosis: current techniques, spectrum of findings, and diagnostic pitfalls. Radiographics. 2006; 26(Suppl 1):S19–41. discussion S42-13. [PubMed: 17050515]

Liu J, Liu T, de Rochefort L, Ledoux J, Khalidov I, Chen W, Tsiouris AJ, Wisnieff C, Spincemaille P, Prince MR, Wang Y. Morphology enabled dipole inversion for quantitative susceptibility mapping using structural consistency between the magnitude image and the susceptibility map. Neuroimage. 2012; 59:2560–2568. [PubMed: 21925276]

Liu P, Xu F, Lu H. Test-retest reproducibility of a rapid method to measure brain oxygen metabolism. Magn Reson Med. 2013; 69:675–681. [PubMed: 22517498]

Liu T, Khalidov I, de Rochefort L, Spincemaille P, Liu J, Tsiouris AJ, Wang Y. A novel background field removal method for MRI using projection onto dipole fields (PDF). NMR Biomed. 2011; 24:1129–1136. [PubMed: 21387445]

Lu H, Clingman C, Golay X, van Zijl PC. Determining the longitudinal relaxation time (T1) of blood at 3.0 Tesla. Magn Reson Med. 2004; 52:679–682. [PubMed: 15334591]

Lu H, Ge Y. Quantitative evaluation of oxygenation in venous vessels using T2-Relaxation-Under-Spin-Tagging MRI. Magn Reson Med. 2008; 60:357–363. [PubMed: 18666116]

Lu H, Xu F, Grgac K, Liu P, Qin Q, van Zijl P. Calibration and validation of TRUST MRI for the estimation of cerebral blood oxygenation. Magn Reson Med. 2012; 67:42–49. [PubMed: 21590721]

Magistretti PJ, Pellerin L. Cellular mechanisms of brain energy metabolism. Relevance to functional brain imaging and to neurodegenerative disorders. Ann N Y Acad Sci. 1996; 777:380–387. [PubMed: 8624117]

McKay LC, Evans KC, Frackowiak RS, Corfield DR. Neural correlates of voluntary breathing in humans. J Appl Physiol (1985). 2003; 95:1170–1178. [PubMed: 12754178]

Poulin MJ, Liang PJ, Robbins PA. Fast and slow components of cerebral blood flow response to step decreases in end-tidal PCO2 in humans. J Appl Physiol (1985). 1998; 85:388–397. [PubMed: 9688710]

Rauscher A, Sedlacik J, Barth M, Haacke EM, Reichenbach JR. Nonnvasive assessment of vascular architecture and function during modulated blood oxygenation using susceptibility weighted magnetic resonance imaging. Magn Reson Med. 2005; 54:87–95. [PubMed: 15968657]

Rodgers ZB, Jain V, Englund EK, Langham MC, Wehrli FW. High temporal resolution MRI quantification of global cerebral metabolic rate of oxygen consumption in response to apneic challenge. J Cereb Blood Flow Metab. 2013; 33:1514–1522. [PubMed: 23838827]

Rostrup E, Law I, Blinkenberg M, Larsson HB, Born AP, Holm S, Paulson OB. Regional differences in the CBF and BOLD responses to hypercapnia: a combined PET and fMRI study. Neuroimage. 2000; 11:87–97. [PubMed: 10679182]

Schweser, F.; Atterbury, M.; Deistung, A.; Lehr, BW.; Sommer, K.; Reichenbach, JR. Proc Int Soc Magn Reson Med. Montreal, Quebec, Canada: 2011a. Harmonic phase subtraction methods are prone to B1 background components; p. 2657

Schweser F, Deistung A, Lehr BW, Reichenbach JR. Quantitative imaging of intrinsic magnetic tissue properties using MRI signal phase: an approach to in vivo brain iron metabolism? Neuroimage. 2011b; 54:2789–2807. [PubMed: 21040794]

Sedlacik J, Kutschbach C, Rauscher A, Deistung A, Reichenbach JR. Investigation of the influence of carbon dioxide concentrations on cerebral physiology by susceptibility-weighted magnetic resonance imaging (SWI). Neuroimage. 2008; 43:36–43. [PubMed: 18678260]

Severinghaus JW. Water vapor calibration errors in some capnometers: respiratory conventions misunderstood by manufacturers? Anesthesiology. 1989; 70:996–998. [PubMed: 2499226]

Sicard K, Shen Q, Brevard ME, Sullivan R, Ferris CF, King JA, Duong TQ. Regional cerebral blood flow and BOLD responses in conscious and anesthetized rats under basal and hypercapnic conditions: implications for functional MRI studies. J Cereb Blood Flow Metab. 2003; 23:472–481. [PubMed: 12679724]

Sicard KM, Duong TQ. Effects of hypoxia, hyperoxia, and hypercapnia on baseline and stimulus-evoked BOLD, CBF, and CMRO2 in spontaneously breathing animals. Neuroimage. 2005; 25:850–858. [PubMed: 15808985]

Smith SM. Fast robust automated brain extraction. Hum Brain Mapp. 2002; 17:143–155. [PubMed: 12391568]

Somers VK, Mark AL, Zavala DC, Abboud FM. Contrasting effects of hypoxia and hypercapnia on ventilation and sympathetic activity in humans. J Appl Physiol (1985). 1989; 67:2101–2106. [PubMed: 2513316]

van der Kouwe AJ, Benner T, Salat DH, Fischl B. Brain morphometry with multiecho MPRAGE. Neuroimage. 2008; 40:559–569. [PubMed: 18242102]

van Zijl PC, Eleff SM, Ulatowski JA, Oja JM, Ulug AM, Traystman RJ, Kauppinen RA. Quantitative assessment of blood flow, blood volume and blood oxygenation effects in functional magnetic resonance imaging. Nat Med. 1998; 4:159–167. [PubMed: 9461188]

Villien M, Bouzat P, Rupp T, Robach P, Lamalle L, Tropres I, Esteve F, Krainik A, Levy P, Warnking JM, Verges S. Changes in cerebral blood flow and vasoreactivity to CO2 measured by arterial spin labeling after 6days at 4350m. Neuroimage. 2013; 72:272–279. [PubMed: 23384523]

Weil JV, McCullough RE, Kline JS, Sodal IE. Diminished ventilatory response to hypoxia and hypercapnia after morphine in normal man. N Engl J Med. 1975; 292:1103–1106. [PubMed: 1128555]

Weisskoff RM, Kiihne S. Mri Susceptometry - Image-Based Measurement of Absolute Susceptibility of Mr Contrast Agents and Human Blood. Magnetic Resonance in Medicine. 1992; 24:375–383. [PubMed: 1569876]

Wong, EC.; Guo, J. Proc Int Soc Magn Reson Med. Salt Lake City, UT: 2013. VENTI: Venous Territory Imaging using Remote Sensing; p. 103

Wu B, Li W, Avram AV, Gho SM, Liu C. Fast and tissue-optimized mapping of magnetic susceptibility and T2* with multi-echo and multi-shot spirals. Neuroimage. 2012; 59:297–305. [PubMed: 21784162]

Wu WC, Fernandez-Seara M, Detre JA, Wehrli FW, Wang J. A theoretical and experimental investigation of the tagging efficiency of pseudocontinuous arterial spin labeling. Magn Reson Med. 2007; 58:1020–1027. [PubMed: 17969096]

Xu B, Liu T, Spincemaille P, Prince M, Wang Y. Flow compensated quantitative susceptibility mapping for venous oxygenation imaging. Magn Reson Med. 2013

Xu F, Uh J, Brier MR, Hart J Jr, Yezhuvath US, Gu H, Yang Y, Lu H. The influence of carbon dioxide on brain activity and metabolism in conscious humans. J Cereb Blood Flow Metab. 2011; 31:58–67. [PubMed: 20842164]

Xu G, Rowley HA, Wu G, Alsop DC, Shankaranarayanan A, Dowling M, Christian BT, Oakes TR, Johnson SC. Reliability and precision of pseudo-continuous arterial spin labeling perfusion MRI on 3.0 T and comparison with 15O-water PET in elderly subjects at risk for Alzheimer's disease. NMR Biomed. 2010; 23:286–293. [PubMed: 19953503]

Highlights

- There is an unmet clinical need for noninvasive oxygenation imaging in the brain.
- We tested a new quantitative susceptibility MRI method to measure regional cerebral oxygenation.
- We measured reduced oxygen extraction fraction during hypercapnic challenge in cerebral veins.
- Oxygenation changes correlated with changes in end-tidal CO_2 in subjects.
- Oxygenation changes related with predicted changes made from separate perfusion MRI measures.

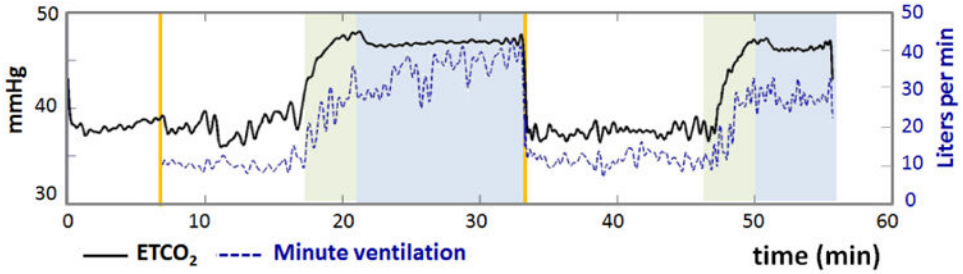

Figure 1.

Physiological time courses of end-tidal CO_2 ($ETCO_2$) in mmHg and minute ventilation in L/min for one healthy subject. Green regions indicate transition periods (~4 minutes) between eucapnia and hypercapnia, and blue regions indicate periods of stable hypercapnia. As expected, $ETCO_2$ increased during hypercapnia and was associated with an increase in minute ventilation.

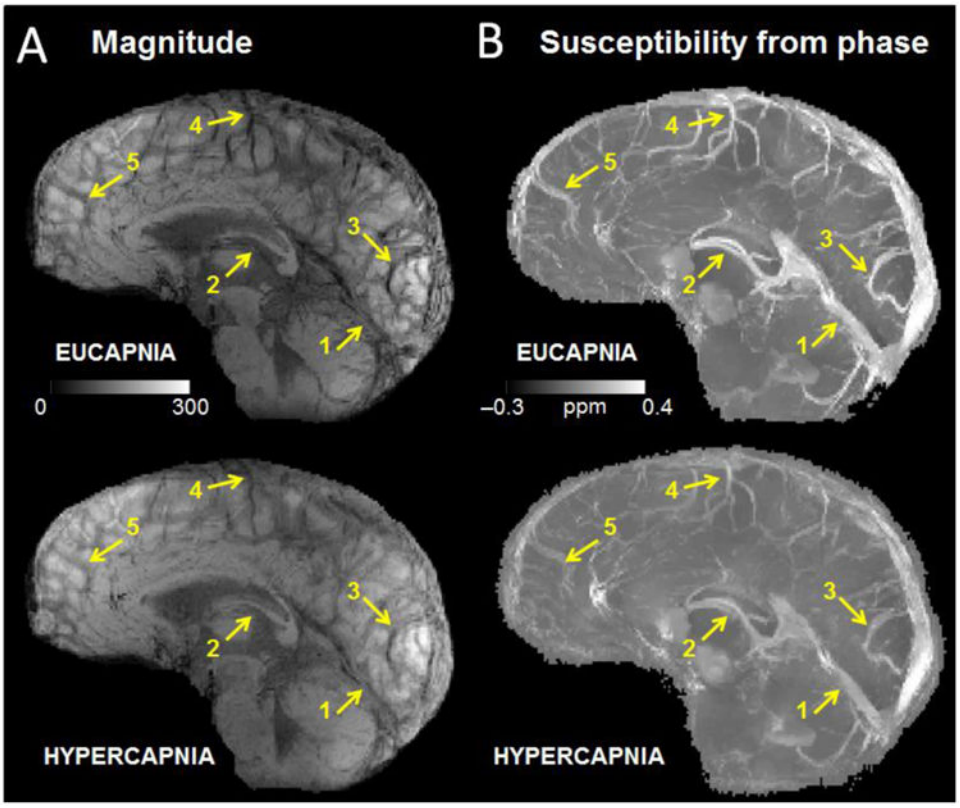

Figure 2.

(a) Minimum intensity projection of gradient echo magnitude images and **(b)** maximum intensity projections of quantitative susceptibility maps (ppm) over 20-mm corresponding to eucapnia and hypercapnia in one subject. Notice the diminished vessel contrast due to decreased venous blood susceptibility during the hypercapnic condition relative to the eucapnic condition on both magnitude and susceptibility images. Yellow arrows indicate individual vessels of interest including (1) the straight sinus, (2) the internal cerebral veins, (3) occipital pial veins, (4) parietal pial veins, and (5) frontal pial veins.

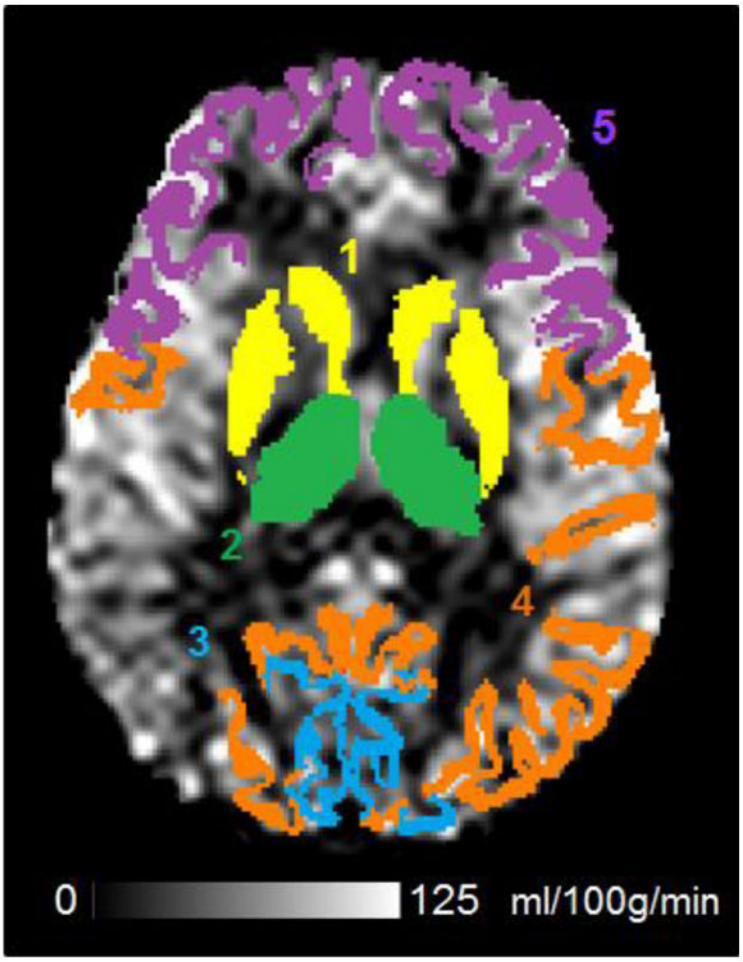

Figure 3.

Regions of interest (ROI) defined from Freesurfer (http://surfer.nmr.mgh.harvard.edu) cortical segmentation for quantification of local cerebral blood flow (CBF) on arterial spin labeling data in one healthy subject. The regions correspond to (1) deep gray matter, (2) thalamus, (3) occipital cortex, (4) parietal cortex, and (5) frontal cortex. The thalami (2) were also included in quantification of regional CBF in the deep gray matter.

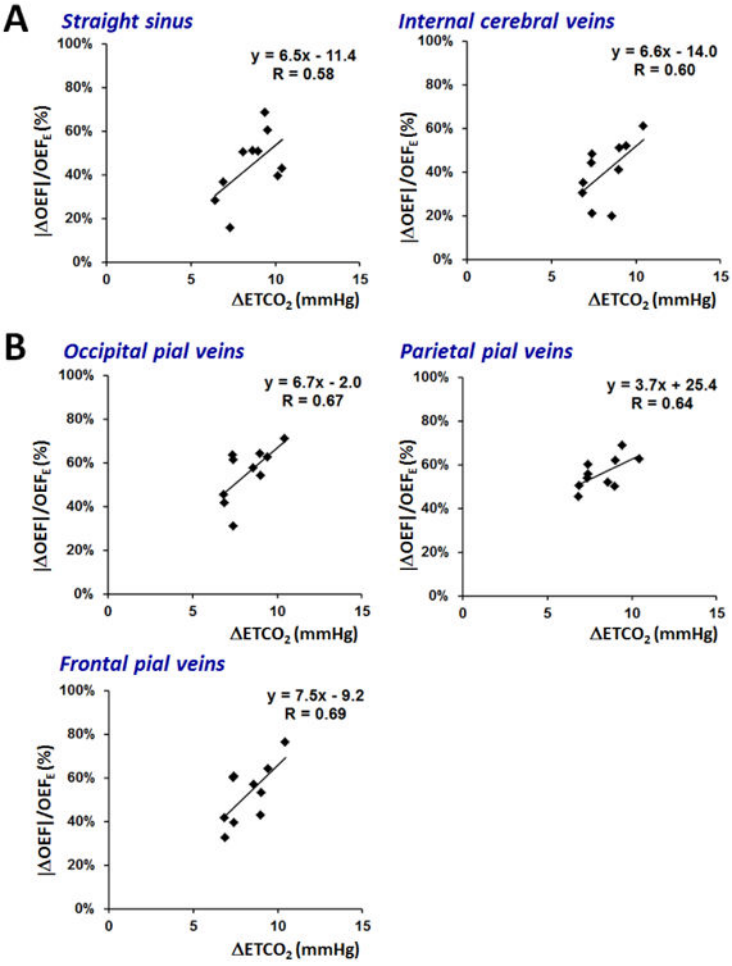

Figure 4.

Scatter plots across subjects of normalized % change in oxygen extraction fraction (OEF) versus increase in end-tidal CO_2 ($ETCO_2$) in mmHg. The plots are generated separately for (a) the straight sinus and internal cerebral veins draining deep gray matter; and (b) cortical pial vessels draining surface gray matter. Linear fits are shown for each graph with slope (% OEF/mmHg) indicating reactivity of vessel OEF to the hypercapnic challenge, and R value to characterize the goodness of fit.

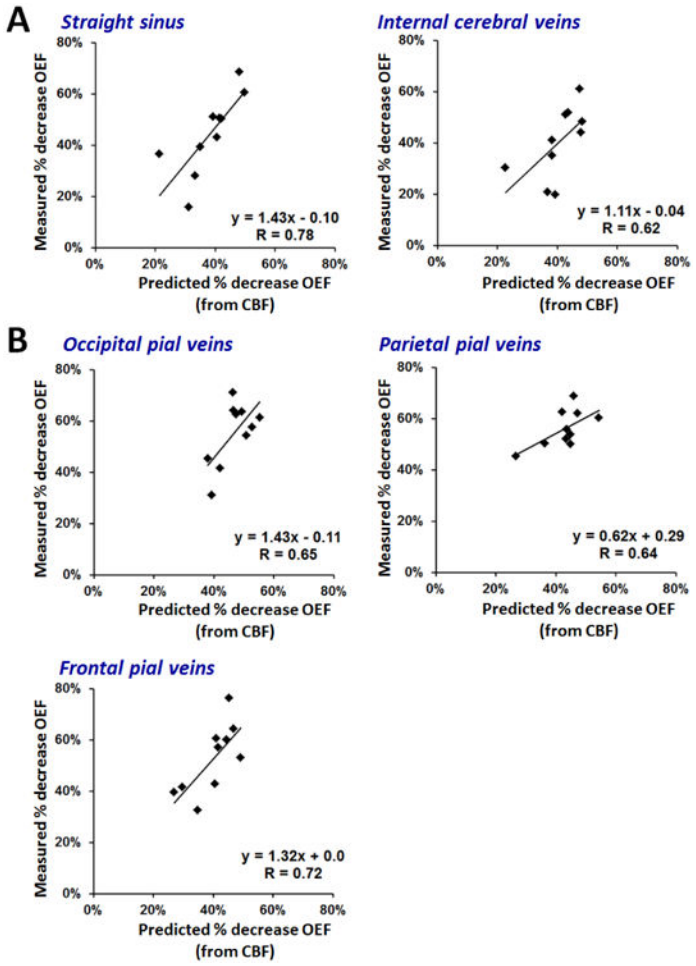

Figure 5.

Scatter plots across subjects of measured versus predicted percent change of oxygen extraction fraction (OEF) in (a) deep gray matter, and in (b) superficial cortical regions. Measured OEF values (vertical axis) derive from susceptibility measurements in individual veins; while the OEF predictions (horizontal axis) are determined solely by cerebral blood flow (CBF) values from the arterial spin labeling acquisitions. Linear fits are shown for each graph with slope with R value to characterize the goodness of fit.

Table 1

Mean and standard deviation of cortical physiological parameters measured by MRI in each gas condition (*N* = 10)

Region	Eucapnia	Hypercapnia	Relative Change (%)
Cerebral Blood Flow – CBF (ml/100g/min)			
Deep gray	42.4 ± 4	69.1 ± 7	64.5 ± 22 *
Thalamus	43.8 ± 5	74.2 ± 9	70.4 ± 20 *
Occipital	47.0 ± 3	89.2 ± 12	89.7 ± 20 *
Parietal	46.0 ± 6	81.4 ± 11	77.5 ± 21 *
Frontal	51.7 ± 6	87.0 ± 11	69.0 ± 20 *
Oxygen Extraction Fraction (%)			
Straight sinus	26.2 ± 5	14.6 ± 5	-42.2 ± 15 *
Internal cerebral veins	30.1 ± 6	18.1 ± 6	-39.9 ± 14 *
Occipital pial veins	27.5 ± 3	12.5 ± 5	-54.6 ± 12 *
Parietal pial veins	31.6 ± 4	14.0 ± 3	-55.7 ± 7 *
Frontal pial veins	28.5 ± 4	13.6 ± 5	-52.3 ± 13 *

* paired t-test *P*-value < 0.001